NJC

New Journal of Chemistry

A journal for new directions in chemistry

Accepted Manuscript

This article can be cited before page numbers have been issued, to do this please use: J. Castillo-Rodriguez, P. D. Ortiz, M. Isaacs Casanova, N. P. Martínez, J. O'Shea, J. Hart, R. Temperton, X. Zarate, D. Contreras and E. Schott, *New J. Chem.*, 2020, DOI: 10.1039/D0NJ03250F.

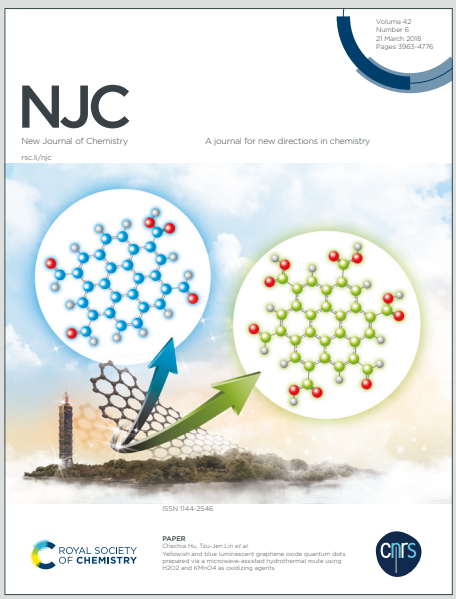

View Article Online
DOI: 10.1039/D0NJ03250F

ARTICLE

Highly Efficient Hydrogen Evolution Reaction, Plasmon-Enhanced by AuNP-L-TiO_2NP photocatalysts

Received 00th January 20xx,
Accepted 00th January 20xx

DOI: 10.1039/x0xx00000x

Judith Castillo-Rodriguez,[a,b] Pedro D. Ortiz,[a*] Mauricio Issacs,[a] Natalia P. Martinez,[a] James N. O'Shea,[b] Jack Hart,[b] Robert Temperton,[b] Ximena Zarate,[c] David Contreras,[d] Eduardo Schott[a,e*]

A set of AuNPs-L-TiO_2NPs nanoaggregates which showed efficient covering of the semiconductor's surface by the AuNPs, as well as appropriate AuNPs sizes for effective sensibilization were use as photocatalyst for the hydrogen evolution reaction (HER). Three aliphatic short-chain linkers: 3-mercaptopropionic acid (MPA), thioglycolic acid (TGA) and thiolactic acid (TLA) were used as stabilizing agent. The slight structure variations of the linkers did not produce differences on the AuNPs size and morphology. However, it was interesting to show how the photocatalytic performance of the nanoaggregates is dependent on the linker present, as well as to determine the influence of the Au/TiO_2 ratio. It was found that TGA gave the best performance at longer irradiation time, though high amounts of H_2 were also obtained for the other two linkers. Furthermore, for all samples large amounts of hydrogen were obtained, which are significantly higher than the usually obtained with plasmon-sensitized TiO_2 nanostructures. In addition, high amounts of H_2 were obtained after five catalytic cycles for all samples, showing the suitability of these nanoaggregates for the photoinduced HER.

1. Introduction

Great efforts have been made to create a system capable of producing alternative fuels using sunlight. To reach a better performance of these systems it is necessary to develop materials that can efficiently absorb and convert sunlight to energy. These materials can be effectively integrated with catalysts that promote the production of fuel. The production of hydrogen gas from solar-driven water splitting processes is one of the most prevalent examples in scientific literature.[1]

However, the water splitting reaction is thermodynamically unfavourable as it requires more than 118.6 kJ/mol (28.4 kcal/mol, 1.23 eV) to happen,[2] which means high overpotentials. From a kinetic point of view, the situation is not better: photocatalytic water splitting is a multi-step process and some of those steps are not rate favourable. Water oxidation, an oxygen evolution reaction (OER), is five orders of magnitude slower than the parallel water reduction, a hydrogen-evolution reaction (HER).[3] Hence, OER is even more difficult than the HER, because OER requires 4 holes (h^+) to occur, while only 2 electrons (e^-) are needed for HER.

The photocatalytic process that can drive the mentioned reactions, *i.e*. OER and HER, can be divided into the following main steps: a) photon absorption, b) exciton separation, c) charge diffusion and transport, d) catalytic reaction on the active site, and e) mass transfer of reactants and products.[4] In step b, semiconductors like TiO_2 are capable of converting an absorbed photon into an electron/hole (e^-/h^+) pair. In photocatalytic water splitting these electrons (e^-) drive the HER, whereas the created holes (h^+) drive OER.[5] Systems for photocatalytic-driven water splitting are desired to be efficient, robust, affordable, and safe.[6] In terms of a suitable photocatalytic system, TiO_2 is both stable and inexpensive. However, it can only harvest photons from the UV spectrum due to its bandgap energy (3.0 to 3.2 eV),[7] which corresponds to a $\lambda_{excitation} \sim 390$ nm. Taking the solar-to-hydrogen (STH) conversion efficiency as a parameter to quantify the H_2-energy generated by solar irradiance, for the National Renewable Energy Laboratory (NREL) standard spectrum of AM 1.5G[8] and using a single semiconductor, just a 3.3% of STH efficiency can be reached for UV photons, whereas the efficiency grows to >17.87% if the visible region (up to 600 nm) is also considered.[9] Therefore, TiO_2 (as well as the majority of semiconductors) does not fulfil effectively the required photon absorption. Besides that, the minority carrier distance (*L*) of many semiconductors useful for water splitting is smaller than their physical dimensions, hence, undesired charge recombination of electrons and holes takes place (Steps b and c).

On the other hand, plasmonics are systems that perform surface plasmon resonance (SPR) when interacting with certain frequency of light. Plasmonic nanoparticles traditionally consist of a noble metal[10] or combinations of them.[11] In recent years plasmonic materials have been combined with semiconductors[12] and graphene.[13] Moreover, a new family of materials has been recently generated, known as active plasmonics,[14] constituted by plasmonic metals and particular types of active surrounding media, such as liquid crystals[15] and dye molecules.[16] SPR refers to the electromagnetic wave-induced collective oscillation of charge carriers in a plasmonic structure. This oscillation can be confined on a subwavelength structure, producing localized surface plasmon resonance (LSPR). LSPR creates an intense electric field and a high degree of light scattering around the nanoparticle,[17] and improves the photocurrent generation of nanoparticle-decorated semiconductor nanosystems.[18] In case of

[a.] *Departamento de Química Inorgánica, Facultad de Química y Farmacia, Centro de Energía UC, Centro de Investigación en Nanotecnología y Materiales Avanzados CIEN-UC, Pontificia Universidad Católica de Chile, Avenida Vicuña Mackenna, 4860, Santiago, Chile.*
[b.] *School of Physics and Astronomy, University of Nottingham, Nottingham NG7 2RD, United Kingdom.*
[c.] *Instituto de Ciencias Químicas Aplicadas, Facultad de Ingeniería, Universidad Autónoma de Chile, Av. Pedro de Valdivia 425, Santiago 7500912, Chile.Address here.*
[d.] *Department of Analytical and Inorganic Chemistry, Faculty of Chemical Science, Universidad de Concepción, Chile.*
[e.] *Millenium Nuclei on Catalytic Processes towards Sustainable Chemistry (CSC), Chile.*

** Authors to whom correspondence should be sent.*
P. D. Ortiz: pdortiz@gmail.com; E. Schott: maschotte@gmail.com.

gold nanoparticles (AuNPs), light absorption occurs at visible wavelengths,[19] allowing applications in a wide range of disciplines, including photoelectrochemical devices,[20] chemistry,[21] energy,[22] sensing systems,[23] and biomedicine.[24] It is important to consider that the LSPR frequency is a function of size and shape of the AuNPs, and it can be tailored according to requirements.[25]

Plasmonics nanoparticles decorating the surface of semiconductors (SC) have been employed in order to overtake their drawbacks, concerning light absorption scope, thus improving their performance in photocatalytic devices.[26] A schematic representation of this situation in case of AuNP-decorated TiO_2 in HER is depicted in Figure 1. Regarding the latter, AuNPs (in general plasmonic nanoparticles) can mainly i) sensitize a semiconductor injecting excited electrons into the conduction band of the TiO_2 (1); and ii) act as an antenna that localizes and transfers the optical energy to the SC, hence, the radiation absorbed is confined to the near-surface region of the semiconductor close to the AuNPs (2), this way making *L* shorter. Therefore, both surface and bulk charge recombination processes (3 and 4, respectively) are minimized.[27]

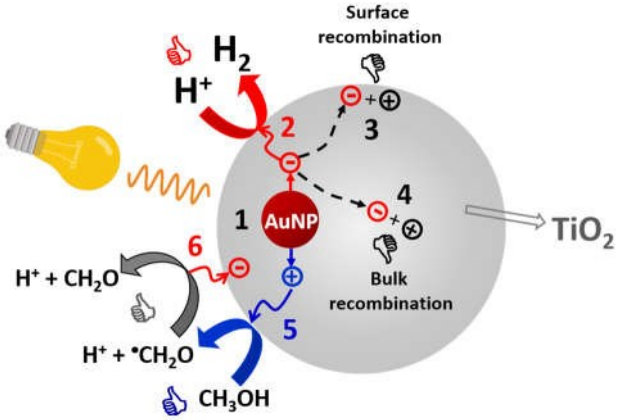

Figure 1 Schematic representation of the plasmonic enhancing effect on the photocatalytic activity of TiO_2 in HER.

In addition, it has been reported that AuNPs-decoration of TiO_2 assisted by linker led to an increase in the photocatalytic activity of the resulting system in comparison to a TiO_2 directly decorated with Au nanoparticles.[28]

In a previous work, we reported the synthesis of gold nanoparticles-linker-TiO_2 nanoparticles nanoaggregates (AuNPs-L-TiO_2NPs), employing a novel variant[29] of the Brust-Shiffrin approach.[30] The as-prepared nanoaggregates showed an efficient covering of the semiconductor's surface by the AuNPs, as well as appropriate AuNPs sizes for effective sensibilization. Three aliphatic short-chain linkers were used as stabilizing agent: 3-mercaptopropionic acid (MPA), 2-mercaptopropionic acid known as thioglycolic acid (TGA) and mercaptoacetic acid or known as thiolactic acid (TLA). However, no significant morphological differences were found for the same Au:linker proportions.[29] It is worth to highlight that in all cases the as-prepared nanoaggregates showed an efficient covering of the semiconductor's surface by the AuNPs, as well as high quality AuNPs regarding morphology and light harvesting properties. In consequence, an effective sensibilization of the semiconductor is achieved. In the herein work, these materials are employed for hydrogen gas evolution toward a photo-induced reaction. Since the AuNPs in the nanoaggregates are connected to the TiO_2 surface by the linker molecules, the performance of the nanoparticles as co-catalyst could be affected by the capacity of the corresponding molecule to carry the charge carriers between the AuNP and the semiconductor. This is a crucial step to improving the necessary charge separation. It has been stablished that electron-transfer rates of the linkers used herein (MPA, TGA, and TLA) are quite different despite the similarity of their molecular structures.[31]

No significant variations in size and morphologies were found in AuNPs obtained employing the linkers for the same Au-toTiO_2 ratios. However, it was interesting to show how the photocatalytic activity of these materials could be dependent on i) the linker present in each (especially regarding electronic criteria), ii) the Au/TiO_2 ratio, iii) the AuNPs size, as well as iv) the covering degree of the SC surface by AuNPs. Finally, reusing cycles were carried out to test the stability of these materials.

The combination of the light harvesting properties of the AuNPs (specially within visible region of the spectrum) and the efficient decoration of the semiconductor surface, makes these nanoaggregates good candidates as high-performance photocatalysts. The later was demonstrated in the herein work for the photocatalyzed HER under visible light.

2. Experimental section

2.1 Materials

AuNPs-L-TiO_2NPs catalysts were prepared according to a variant of Brust-Schiffrin approach, previously reported by our group.[29] Briefly, 50 mg of commercial TiO_2 (Degussa P25, ≥ 99%, Merck) was dispersed by sonication in 50 mL of acidified Milli-Q water (pH = 1.69, 85 µL of concentrated HCl). Then, 30 mmol of thiol was added and the mixture was kept under vigorous stirring for 30 min. The resulting mixture was then centrifuged, and the solid was washed with Milli-Q water (3 × 10 mL), in order to eliminate the remaining free thiol molecules. The resulting solid was re-dispersed by sonication in other 50 mL of acidified Milli-Q water (pH = 1.69, 85 µL of concentrated HCl) and placed under vigorous stirring. Then, the corresponding volume of $HAuCl_4$ (30%) was added and the system was stirred for other 20 min. Then, the mixture was cooled to 2-4 °C in an ice bath and the corresponding quantity of $NaBH_4$ was added. Vigorous stirring at 2-4 °C was kept for 1 h. The resulting AuNP-L-TiO_2NPs were isolated by centrifugation, washed with Milli-Q water (3 × 10 mL) and dried overnight in vacuum at 50 °C.

Bottles and magnetic stirrer bars were exhaustively cleaned with freshly prepared *aqua regia* solution, rinsed with Milli-Q water, and dried before using them. Methanol, HNO_3, and HCl (all of analytic grade) were purchased from Merck and employed with no further treatment.

2.2 Methods

2.2.1 UV-Vis characterization

UV-Vis spectrum of each AuNPs-L-TiO_2NPs nanoaggregate was recorded in diffuse reflectance mode (DRS) in a Cary Series UV-Vis-NIR spectrophotometer. The band gap energies (*Eg*) were calculated from these data, employing the Kubelka–Munk function for diffuse reflectance: $f(R) = (1-R)^2/(2R)$ and Tauc plot method. Since TiO_2 is an indirect semiconductor, the final equation to use in the linear region of the function is $[f(R)h\nu]^{1/2} = K(h\nu - Eg)$ and the respective band gaps (*Eg*) were obtained by extrapolating to zero.

View Article Online
DOI: 10.1039/D0NJ03250F

2.2.2 Samples preparation for photocatalysis

To prepare each sample, 4 mg of the corresponding AuNPs-L-TiO_2NPs and 3 mL of a freshly prepared water/methanol solution (9:1 v/v) were introduced in a 10 mL bottle. The mixture was sonicated to obtain a well-dispersed suspension. After that, the resulting suspension was degassed with N_2 to remove dissolved gasses, sealed, and protected from light. A magnetic stirrer bar was added before sealing the bottle. Every sample was sonicated again before the irradiation assays.

2.2.3 Photocatalytic hydrogen production

The as-prepared samples were irradiated employing a simulated sunlight source provided by Arc Lamp Power supply (Oriel Co) 150W Xe/200W HgXe. Stirring was maintained during the process in order to improve the homogeneity of the system, as well as to avoid generated hydrogen gas to remain physiosorbed on the catalyst surface.

After the corresponding irradiation time, 40.0 μL of gas were collected from the headspace reactor by a syringe, and injected directly on a DANI MASTERS GC, with a fused silica capillary column (Supelco Mol Sieve 5A plot, 30 m × 0.53 mm) coupled with a micro thermal conductivity detector (μTCD) using argon as carrier gas. For every measurement, the syringe was previously cleaned with N_2 purge (10 min) and checked by measuring 40 μL of N_2. The amounts of hydrogen gas (μmol) were quantified by calibration curve (from 2 μL to 50 μL of pure gas) using the ideal gas equation. The calibration curve was accomplished in duplicate. The coefficient correlation (R^2) obtained was 0.999.

2.2.4 Catalyst reuse cycles

For each cycle of recycling the sample preparation described above was accomplished. Between cycles, the solid was separated by centrifugation, dry under vacuum, and the preparation was repeated. An irradiation time of 60 min was selected and the rest of irradiation conditions were the same as previously described. Five reusing cycles were performed.

2.2.5 XPS analysis

Experiments were carried out at the "Hippolyta" Devi-sim (SPECS) near ambient pressure X-ray Photoelectron Spectroscopy (XPS) instrument (University of Nottingham). The samples were prepared by pressing the powder into carbon adhesive pads. Measurements were taken in ultra-high vacuum using the Phoibos 150 hemispherical analyzer, monochromatic Al Kα x-rays (hν = 1486.6 eV) and the low energy electron flood gun for charge compensation. Binding energy scales were calibrated by Ti 2*p* at 458.5 eV. After subtraction of a Shirley background, peak fitting was done using pseudo-voigt functions with 0.9 gaussain and 0.3 lorensian components.

3. Results and Discussion

3.1 Synthesis of the AuNPs-L-TiO_2NPs catalysts

AuNPs-L-TiO_2NPs catalysts were prepared following an alternative procedure based on a one-face aqueous Brust-Schiffrin approach. The size of the AuNPs in the nanoaggregate were dependent on the Au:stabilization-agent molar ratio, whereas it was independent from the linker used in each case. Thus, three main diameters (≤ 1.0 nm, ~ 3.5 nm, and ~ 4.5 nm) were detected, depending on the Au:stabilization-agent molar ratio.

Details regarding morphological and physicochemical characterization of the nanoaggregates can be found in a previous work. Briefly, it is worth to highlight that spherical-shaped and homogeneous in size AuNPs were obtained, as can be appreciated in TEM and HRTEM (as inset) micrographs of **G6** shown in Figure 2A. The XRD diffractograms of **G6** and **G8** can be seem in Figure 2B. The main diffraction peaks expected are present, *i.e.* Au(111), anatase (101) and rutile (110). In addition, the crystalline structure of Au in the nanoparticles is also appreciated in the HRTEM micrograph (inset in Figure 2A) and the corresponding detected from live Fast Fourier Transform.[29]

It is interesting to check if the different structures of the three linkers could affect the photo-catalytic properties of the nanoaggregates in a H_2 evolution photoreaction. Hence, three proportions were used

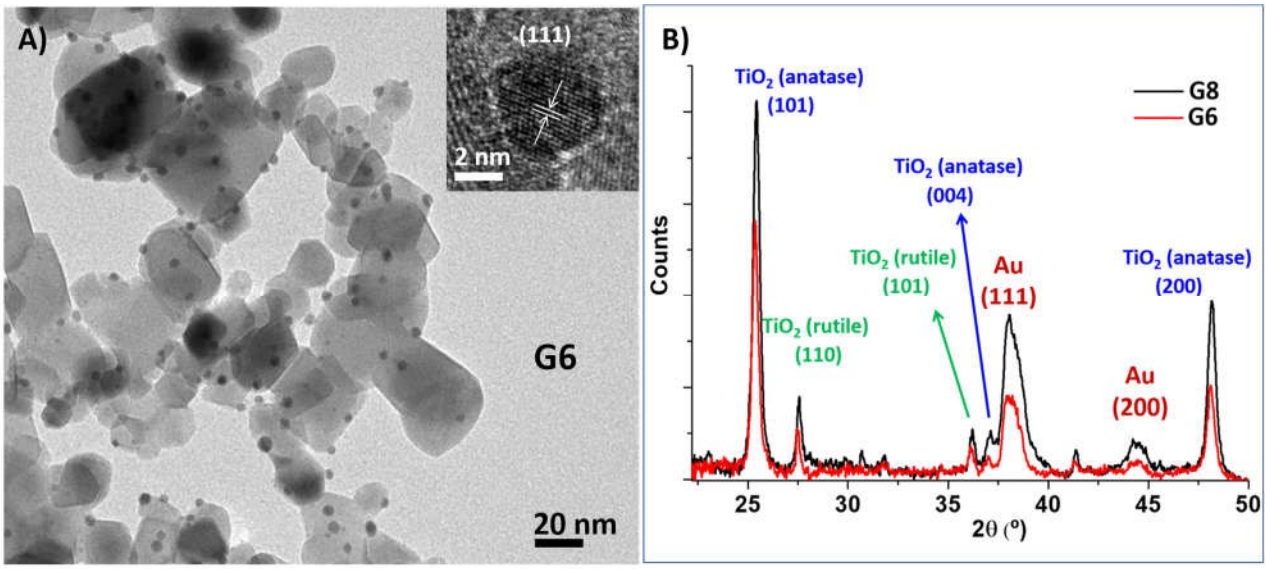

Figure 2 A) TEM and HRTEM (as inset) micrograph, and B) XRD diffractogram of AuNPs-decorated TiO_2 nanoaggregates.[29]

on the catalytic trials, each one from the three different main diameters, respectively. In Table 1 the Au/TiO_2 % in weight, the corresponding linker, and main diameter for the AuNP-L-TiO_2 nanoaggregates employed as photocatalyst are summarized.

Table 1. Nomenclature, Au/TiO_2 % in weight, linker, and main diameter for each photocatalyst.

Nomenclature	Au/TiO_2 (w:w %)	Linker	Main diameter (nm)
M2	2.0	MPA[a]	≤ 1.0
M6	5.0	MPA[a]	~ 3.5
M8	10.0	MPA[a]	~ 4.5
L2	2.0	TLA[b]	≤ 1.0
L6	5.0	TLA[b]	~ 3.5
L8	10.0	TLA[b]	~ 4.5
G2	2.0	TGA[c]	≤ 1.0
G6	5.0	TGA[c]	~ 3.5
G8	10.0	TGA[c]	~ 4.5

[a] 3-mercaptopropionic acid; [b] thiolactic acid; [c] thioglycolic acid

3.2 Hydrogen evolution photoreaction

For each linker a sample from each of the three different AuNPs size distribution was employed as catalyst in the photocatalytic HER. As this is a reductive process, it is convenient the addition of a sacrificial electron donor.[32] Thus, in the present study methanol was used as the sacrificial reducing agent. It has been proposed that primary alcohols with α-hydrogen react with holes (h^+) producing protons (H^+) and the corresponding hydroxyalkyl radical intermediate, according to Equation 1 (see process 5 in Figure 1). This intermediate possesses enough energy to produce H^+, the respective aldehyde, and one electron (Equation 2, also see process 6 in Figure 1).

$$CH_3OH + h^+ \rightarrow {}^{\bullet}CH_2OH + H^+ \qquad \text{Eq. 1}$$

$$^{\bullet}CH_2OH \rightarrow CH_2O + H^+ + e^- \qquad \text{Eq. 2}$$

This electron can be injected into the TiO_2 conduction band, improving the number of charge carriers. The last has been called the current doubling effect. Finally, generated H^+ can react with electrons to produce H_2.[33] In the presence of a hole scavenger like methanol, the lifetime of the trapped electrons in nanocrystalline TiO_2 is significantly increased. Thereby, by avoiding the undesired electron/hole recombination, methanol increases H_2 evolution rate. Consequently, pure methanol and high proportions of methanol in a hydroalcoholic solution produce larger amounts of H_2 than diluted ones or pure water.[34] However, while this research was focused on employing water as the main source of H^+ ions, H_2O/MeOH (9:1) solution was selected as the reaction media. In fact, no appreciable H_2 was produced in the absence of MeOH, while the rest of conditions remained unchanged. It is also worth to mention that Guzman *et al*. demonstrated via GC-MS measurements for a D_2O/CH_3OH solution (similar in proportion to the one used in this work), that the greater amounts of gas species were D_2 and DH. Moreover, they found that the proportion of H_2 was very low and became even lower in time. It means that water is the main source of H_2 in these conditions.[33]

Regarding the role of Au-TiO_2 system as photocatalyst of H_2 evolution photoreactions, two main approaches have been proposed. One involves the direct photoexcitation of the semiconductor leading to the production of electrons in its CB. These hot electrons are thereupon injected from the CB to the gold nanoparticles acting as catalytic sites for H_2 generation. This is the rational driving path for radiation wavelengths from UV to visible wavelength under the absorption energy of the AuNPs (~ 520 nm for spherical shaped ones).[35] On the other hand, for radiation wavelengths around or higher than the excitation energy of the AuNPs, electrons produced from the photoexcitation of gold are injected into the CB of the semiconductor. The catalytic sites for the photogeneration of H_2 are therefore located on the surface of TiO_2 and close to the AuNPs.[36] In these conditions the necessary synergism between Au and TiO_2 has been verified, while it was found that AuNPs stabilized with citrated lack of photocatalytic activity in H_2 production.[37] Furthermore, in the present research silica-glass bottles were used as reactors, thus radiation of wavelengths under 200 nm were avoided because this material is effective opaque for wavelengths equal and lower than the mentioned value.[38] Despite the band gap of TiO_2 (3.0 to 3.2 eV for the bulk) corresponds to an excitation energy of ~390 nm (it should be noted that this wavelength is even shorter for TiO_2 nanostructures ~350 nm),[39] very low amount of H_2 (in the order of μmol/h) was detected when bare Degussa P25 were employed as the photocatalyst in the same conditions. Therefore, the aforementioned criteria suggest that the AuNPs act as an efficient sensitizer of TiO_2 enhancing the reduction reaction, which produces H_2 on the semiconductor surface. In this sense, three mechanisms have been proposed: i) photoinduced heating of metal NPs;[40] the proper electron transmission from metal NPs to the semiconductor;[41] and iii) enhanced excitation efficiency of the

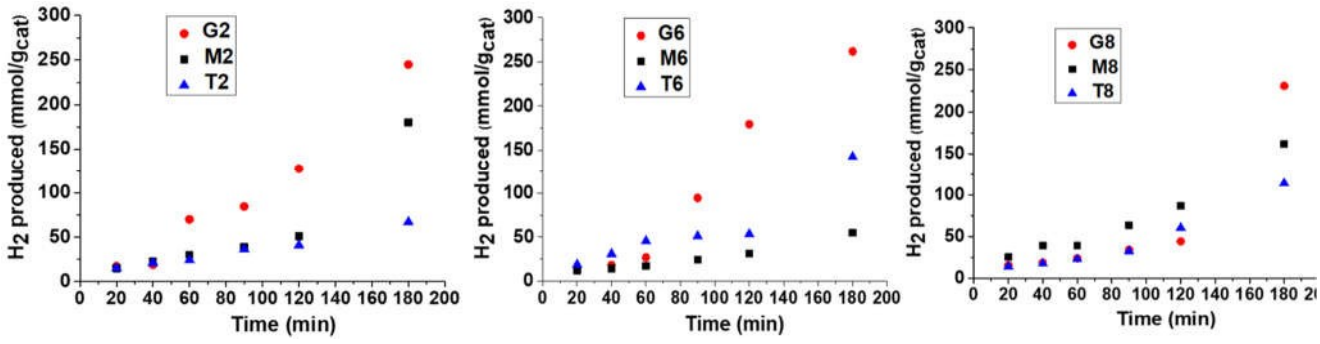

Figure 3 H_2 produced via photochemical reaction, employing the series of AuNP-L-TiO_2NP nanoaggregates as photocatalysts in a H_2O:MeOH (9:1 v/v) solution. Nomenclature employed herein has been declared in Table 1.

semiconductor by the electromagnetic field of the metal NPs.[42] Mechanism iii) is based in
the coupling between the LSPR of the AuNPs and electronic states in the TiO_2, derived from surface defects.[43] For AuNPs, mechanism i) is dismissed since no photocatalytic activity is observed for free AuNPs in the absence of TiO_2.[44] Finally, mechanism ii) is considered the main driving force for the photocatalytic reaction, however, the contribution of mechanism iii) cannot be neglected.[45]

For every photocatalyst system measurements upon 20, 40, 60, 90, 120, and 180 minutes of irradiation were carried out under stirring conditions at room temperature. Results are summarized in the graphics included in Figure 3.

It can be appreciated that the H_2 production profiles obtained were similar for the three proportions series at irradiation times lower that 120 min, regardless of the linker employed. The differences are observed for longer time of irradiation. The largest amount of H_2 gas was obtained when TGA was the linker for the three proportions at the maximum radiation time (180 min). Further on, it is remarkable that in most cases high yield of H_2 were obtained regardless the Au-TiO_2 proportion or the linker employed. Only with **T2** and **M6** the amount of generated H_2 was significantly less than in the rest of the samples. To the best of our knowledge, the amounts of H_2 obtained employing these materials after 180 min of irradiation (~50 - 250 mmol/g_{cat}) are larger than most of the typically obtained with plasmon-decorated TiO_2 nanoparticles, *e. g.*, ~8 mmol/g_{cat},[46] ~45 mmol/g_{cat},[47] and ~60 mmol/g_{cat}.[48] Moreover, a similar ammount of H_2 yields obtained in this work was reported by Rahul *et al* (~120 mmol/g_{cat}), but employing a AuNP-loaded Ti^{3+} self-doped TiO_2 photocatalyst.[49] It has been found that these Ti^{3+} enhance the efficiency of the photocatalysis by reducing the E_g[50] and improving the electron transfer within the crystal lattice of the TiO_2.[51] It is important to remind that in the present study commercial Degussa 25 is employed as TiO_2 with no additional treatment. It is also worth to notice that no saturation behavior was detected for any samples at the larger irradiation time (180 min).

In order to study how the AuNP decorating the surface of the TiO_2 modify the absorption energies of the resulting materials in comparison to bare TiO_2, the band gap was determined for the three proportions employed in the present work. Therefore, diffuse reflectance experiments were carried out and Kubelka–Munk function and Tauc plot method were employed to analyze the obtained data.

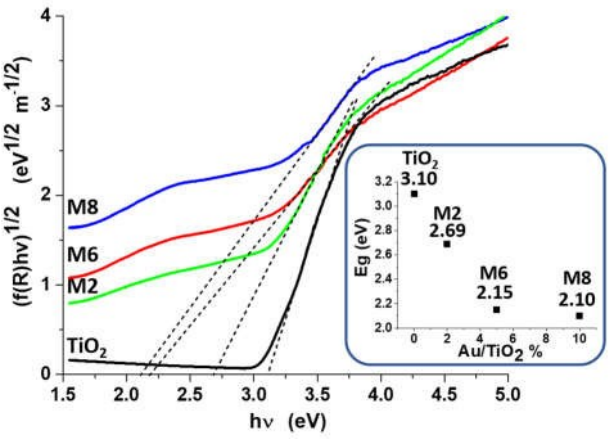

Figure 4 $[f(R)h\nu]^{1/2}$ versus $h\nu$ plots for the series were MPA is the linker and for bare TiO_2 (Degussa P25). Band gab energies (*Eg*) as a function of Au/TiO_2 percent are presented as inset.

The plots of $[f(R)h\nu]^{1/2}$ versus $h\nu$ for the series where MPA is the linker are shown in Figure 4. Here $f(R) = (1-R)^2/(2R)$, where R is the reflectance as a function of the incident radiation energy. In the linear region of the function, the expression $[f(R)h\nu]^{1/2} = K(h\nu - Eg)$ is satisfied, where *Eg* is the band gap energy. Since this method can lead to errors depending on the methodology employed, a fitting was applied in the region were the function is linear. The resulting band gap values are shown as inset in Figure 4.

There is a decrease in *Eg* for all AuNP-L-TiO_2 nanoaggregates compared to bare TiO_2. Furthermore, it can be appreciated that larger Au/TiO_2 % lead to smaller *Eg*. These results suggest that AgNPs actually improve the light absorption capability of the resulting materials compared to bare Degussa P25.[52] In this sense, this reduction was larger for **M6** and **M8** in comparison to **M3**, however, there is just a slight difference between **M6** and **M8**. These lower *Eg* values could be related to a better light harvesting capability and could also be positive for photocatalytic purposes. However, it was found through diffuse reflectance spectroscopy and electronic paramagnetic resonance studies that the number of photogenerated active Ti^{3+} sites in TiO_2 increases linearly with the irradiation time for bare TiO_2, whereas this number remains quite invariable for Pt^0-load TiO_2. This behavior has been explained considering an electron migration from the TiO_2 conduction band to the Pt contact, what apparently contradict Schottky barrier model.[53] It means that an excessive increment in noble metal/TiO_2 percent produces a decrease in the photocatalytic activity. Hence, a compromise between the positive effect of LSPR from noble-metal nanoparticles and the negative secondary electronic migration mentioned above should be tailored. For the series studied herein, better results were obtained for proportion 6 (5%), which are the samples with the intermediate value of Au/TiO_2 % composition.

Another important factor to be considered is the degree of SC surface coverage by AuNPs. As it was demonstrated in a previous work, the surface of TiO_2 in all nanoaggregates employed as photocatalyst in this work is efficiently decorated by AuNPs. Moreover, the highest density of AuNPs coverage was obtained for proportion 2.[29] This factor enhances the catalytic effect of nanoaggregates from proportion 2, while the greater absorption yields improves the activity in the case of other two proportions.

Urbach energies (*Eu*) were also determined to complement the optical characterization of these materials. This parameter is assumed as the width of the absorption tail resulting from localized electronic states lying into the band gap of the semiconductor. The existence of these electronic states is associated to crystal defects, hence, *Eu* have been widely employed to characterize the generation of defects in doped materials.[54] In particular, for doped TiO_2 *Eu* has been related to oxygen defect centers.[55]

Eu can be determined using equation 3:

$$\alpha = \alpha_0 + e^{(\frac{E}{Eu})} \qquad \text{Eq. 3}$$

were α is the absorption coefficient, *E* is hν, and *Eu* is the Urbach energy, respectively.[56] Its value can be obtained as the reciprocal of the slope in the linear fit (below the band gap interval) in the plot of Ln(α) vs. *E*. As it was assumed in the graphic determination of *Eg*, it was used the function *f(R)* instead of α. The plots for the M series samples, as well as *Eu* values are shown in Figure 5.

For the interpretation of these results it is important to remind that Degussa P25 is not a doped TiO_2 and it was employed without further structural lattice modification. In addition, Au atoms (or Au^I ions in case) are not lying as TiO_2 structure dopants. Thus, the generation of aforementioned Ti^{3+}-crystal defects in TiO_2 upon irradiation could be

View Article Online
DOI: 10.1039/D0NJ03250F

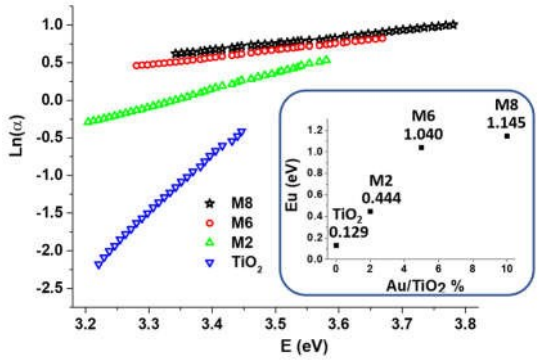

Figure 5 Plots of Ln(*f(R)*) vs. *E* for the series whit MPA as linker. Plot of *Eu* vs. Au/TiO_2% is presented as inset.

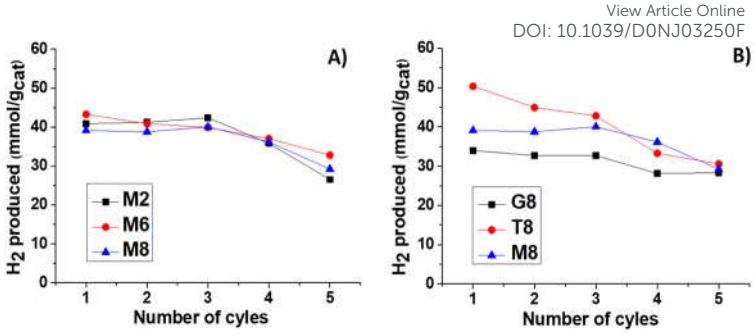

Figure 6 H_2 produced upon five cycles of photocatalysis from A) a series where MPA was the linker on each catalyst, and B) a series where proportion 8 was employed with each linker.

significant for the Au-low-loaded samples from proportion 2 but should not be the single reason of Eu increase form proportion 6. In this sense, it is suitable to think on the contribution of defects into AuNPs crystal structure as an additional contribution. Despite XRD characterization of the series of AuNPs employed in the herein work demonstrated a high degree of crystallinity within the spheres (Au(111) is the majority crystalline phase), nanostructures in general bears a significant proportion of boundary defects as a consequence of the high surface/volume ratio. One possible explanation for the Eu profile found in these materials is that upon the increase in Au%, the impact of the boundary defects also increases. The combination of mentioned factors is proposed as the reason of the raise in Eu value with the increase in Au% observed from bare TiO_2 to samples from proportion 6. However, from proportion 6 to proportion 8, just a slight variation is detected. The negative effect of electronic secondary migration could be the cause of the flatting in the Eu profile.

As it has been shown, the combination of competitive effects could explain the similar results obtained for the three studied proportions in terms of hydrogen produced, despite the differences in AuNPs size and Au/TiO_2 proportions.

3.3 Reusability assays

To test the capacity of the nanoaggregates to remain stable and active upon several photocatalytic processes, five cycles were performed employing the same sample. In every cycle, the irradiation time was 60 min and the same reaction conditions were used. The photocatalyst was exhaustively isolated from the reaction media, washed with Milli-Q water and dry under vacuum before the next use.

In Figure 6 the recycling profiles for two series of photocatalysts are shown. Specifically, in Figure 6A there are shown the results for TMA, when the linker remains unchanged, whereas the Au/TiO_2 % was

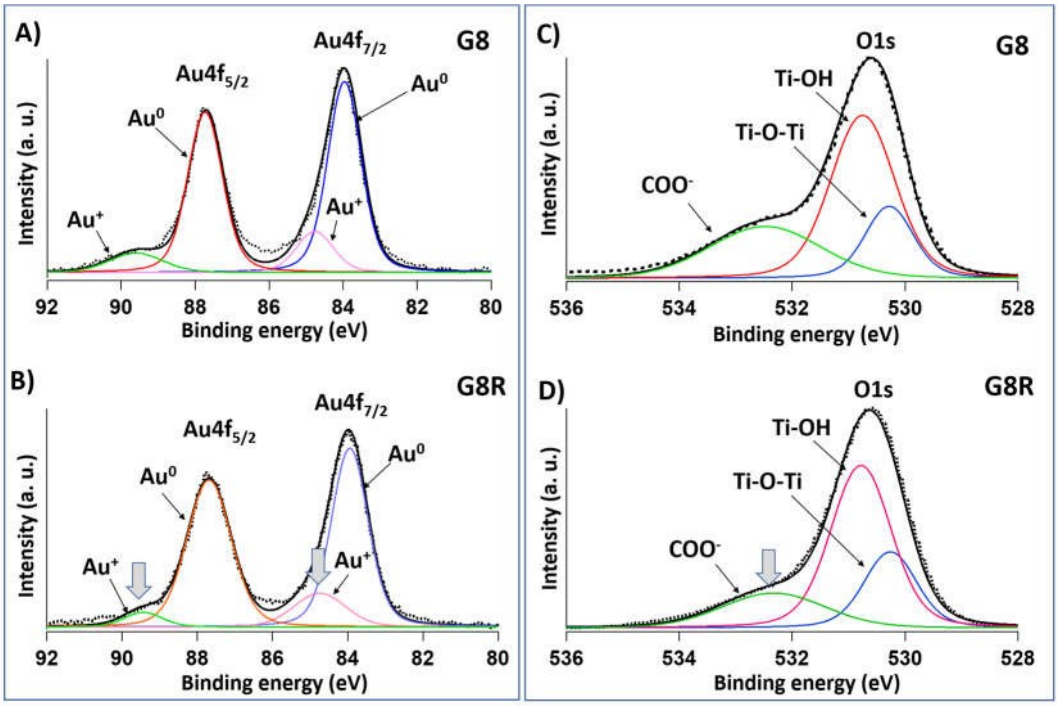

Figure 7 High-resolution XPS corresponding to Au and O regions from **G8** (A and C) and **G8R** (B and D). In the Figure, A) Au 4*f*, C) O 1s from **G8**; and B) Au 4*f*, D) O 1*s* from **G8R**. The slight decrease in intensity of Au^+ and COO^- contributions for **G8R** is highlighted with grey arrows in each case.

changed. On the other hand, in Figure 6B the linker is changed while the proportion Au/TiO_2 % remains unchanged. As can be seen in Figure 6, after three cycles just an appreciable decrease in H_2 production is observed in T8 (15%). Upon five cycles, an average decrease of 28% in MPA series (Figure 6A) and 35% in the proportion 8 series were detected. However, it is important to highlight that large quantities of H_2 are obtained even after 5 cycles.

In order to check grade of photocatalyst degradation, X-ray photoelectron spectroscopy (XPS) spectra were measured for **G8** (the linker with the best performance in HER) before and after carrying out the five reuse cycles. Samples **G8** and **G8R** (**G8R** is **G8** after the five reusing cycles) were selected to carry out XPS due to two main factors: i) this sample shows the best H_2 generation values, and ii) the proportion 8 is the richest sample in Au amount. The amount of Au is important to obtain a better resolution in XPS measurements since the proportion in weight of Au in our samples is very low, which is crucial to measure a signal for the weak peaks from S 2*p*.

In the survey spectra (data not shown) of **G8** and **G8R**, the expected spin-orbit doublet for Ti 2*p*, Au 4*f*, and S 2*p* are present, as well as the signal corresponding to O 1*s*. The most probable sources of degradation in the nanoaggregates should be the breaking of both, the Au-S bond between AuNPs and the linker, and the COO^--Ti bond between the linker and the TiO_2. The XPS analysis will be focused on Au 4*f*, O 1*s* and S 2*p* peaks to use them as indicators of the nanoaggregate stability. All spectra were normalized to the height of the most intense peak in the spectra for comparison purposes.

High-resolution spectra were recorded in the regions of interest for the following analysis and they are shown in Figure 7. For the Au 4*f* spectra both components were deconvoluted into two peaks, as evidence of different chemical environments (see Figure 7A). The peaks from the low binding energy component Au $4f_{7/2}$ appear at 83.95 eV and 84.74 eV, respectively. The first one corresponds to Au^0 from the core of the AuNPs, whereas the second and less intense peak is associated to Au interacting with thiol (Au-S bond).[57] Since this specie results from the interaction of Au with the more electronegative S atom, it bears a positive partial charge and is represented as Au^+. A similar situation is observed for Au $4f_{5/2}$ component.

On the other hand, O 1*s* signal is asymmetric with a wide tail spreading toward higher binding energy values. This peak was fitted to three contributing components at 530.3 (Ti-OH), 530.8 (Ti-O-Ti), and 532.5 eV (COO^-), respectively.[57] The last one corresponds to the carbonate moiety from the linker anchored to the semiconductor surface and will be considered as the second marker for the photocatalyst stability checking.

The third indicator to be considered is the S-Au component in the S 2*p* signal. This signal is a direct evidence of the linker-gold bond formation and, in ideal conditions, it is a key tool for its characterization. However, since the Au/TiO_2 ratio is low, an optimal resolution could not be achieved even for the richest-in-gold proportion (proportion 8). Consequently, the statistical treatment for deconvolution do not apply in this case.

Hence, most of the signal intensity of the three mentioned contributions (Au^+, COO^-, and S-Au) in the corresponding **G8R** spectra is retained, as sign of poor nanoaggregate degradation. From spectrum of **G8R** (see Figure 7B), it is observed an intensity decrease of ~ 13% of the Au^+ signal compared to the spectrum of **G8** (see Figure 7A). A similar situation is appreciated from spectrum of **G8R** in Figure 7D, compared to spectrum of **G8** in Figure 7C, regarding the contribution of COO^-, where ~ 20% of the original intensity is lost.

In Figure 8, S 2*p* spectra of **G8** and **G8R** are shown. The peaks from S 2*p* signals are very week for both samples. The signal at lower binding energy (161.7 eV) correspond to S-Au interaction, while the signal observed at 169.1 eV is assigned to $SO_3^{2-}Na^+$ specie.[58] As can be seen, just slight changes occurred in the sample after the reusing process.

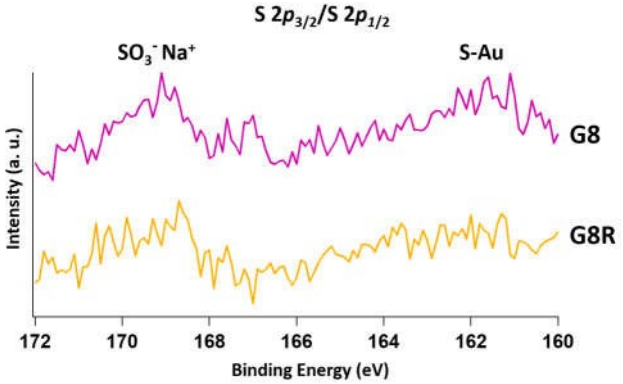

Figure 8 High-resolution XPS corresponding to S 2*p* regions from **G8** and **G8R**.

The qualitative information obtained from this measurement, combined with the data obtained from the other two indicators is reliable to draw a conclusive idea about the nanoaggregate stability. According to the later, it is shown that most of the photocatalyst remains stable after the five reusing cycles of HER. This result agrees with the loss in hydrogen production verified upon the reusing cycles. Despite this grade of photocatalyst deactivation, the amounts of H_2 produced are significative large.

Hence, the AuNP-L-TiO_2NP can be considered as highly efficient photocatalyst for HER and, moreover, it has been shown that they retain most of their activity upon five cycles of reusing.

4. Conclusions

In the current work, high yields in photocatalyzed hydrogen evolution reaction have been achieved using AuNP-L-TiO_2NP nanoaggregates, respect to analogous systems were plasmonic nanoparticles were employed as sensitizers of TiO_2 nanostructures. Hence, these AuNP-L-TiO_2NP nanoaggregates have performed as very active photocatalysts, since an enhancement of the photocatalytic efficiency of the nanoaggregates occurs via the LSPR absorption of the AuNPs.

Significative high amounts of H_2 were obtained regardless both the Au/TiO_2 weight percent (2, 5, 10%) or the short-chain linker (MPA, TLA, TGA) employed. However, at the longest time of irradiation (180 min) the best results were yield when TGA was the linker, especially the sample G6. Better absorption properties were verified in samples with greater proportion of Au, *i.e.* the ones with bigger AuNPs main diameters. On the other hand, a detrimental electron migration from the semiconductor conduction band to noble metal, which increases with the metal/TiO_2 percent, has been claimed as a competitive factor against the photoactivity of the richer-in-gold samples. The greatest covering efficiency of semiconductor surface by AuNPs verified in proportion 2 (smallest metal percent and diameter) is an additional factor that enhances the catalytic activity of the corresponding samples. An equilibrium between the mentioned qualities is proposed herein as a logical explanation for the better results yield for the intermediate proportion 6. Finally, it was verified

that nanoaggregates maintain most of its photocatalytic activity after five photocatalytic reusing cycles, and more important, large amounts of H_2 are produced even in these conditions. The last is crucial for its possible use in the industry.

In summary, these series of nanoaggregates are of high photocatalytic activity, are easy to prepare, can be efficiently recovered after each photocatalytic cycle, and are obtained in aqueous medium, this way avoiding the use of pollutant solvents. For those reasons, these materials can be considered as great candidates to be employed as photocatalysts for the high-efficient photocatalytic production of H_2.

Conflicts of interest

There are no conflicts to declare.

Acknowledgements

Financial support by FONDECYT 1201880, 1180565, ANID/FONDAP/15110019, and CONICYT doctoral fellowship number 21160394 grants is acknowledged. Millennium Science Initiative of the Ministry of Economy, Development and Tourism-Chile grant Nuclei on Catalytic Processes towards Sustainable Chemistry (CSC) is also acknowledged. O'Shea, Temperton and Hart grateful to the Energy Research Accelerator (Innovate UK), the Engineering Physical Sciences Research Council (EPSRC) and the University of Nottingham Propulsion Futures Beacon for funding the XPS measurements.

References

1 P. Ganguly, M. Harb., Z. Cao, L. Cavallo, A. Breen, S. Dervin, D. D. Dionysiou, S. and C. Pillai, *ACS Energy Lett.*, 2019, **4**, 1687-1709.
2 A. Kudo and Y. Miseki, *Chem. Soc. Rev.*, 2009, **38**, 253–278.
3 S. J. Moniz, S. A. Shevlin, D. J. Martin, Z.-X. Guo and J. Tang, *Energy Environ. Sci*., 2015, **8**, 731–759.
4 K. Afroz, M. Moniruddin, N. Bakranov, S. Kudaibergenov, N. Nuraje, *J. Mater. Chem. A*, 2018, **6**, 21696–21718.
5 J. K. Hyung, S. H. Lee, A. A. Upadhye, I. Ro, M. I. Tejedor-Tejedor, M. A. Anderson, W. B. Kim, G. W. Huber, *ACS Nano*, 2014, **8**, 10756–10765.
6 N. S. Lewis, *Science*, 2016, **351**, aad1920 DOI: 10.1126/science.aad1920.
7 K. Sivula, R. van de Krol, *Nat. Rev. Mater.,* **2016**, *1*, 15010.
8 National Renewable Energy Laboratory (NREL). Website: http://rredc.nrel.gov/solar/spectra/am1.5.
9 K. Takanabe, *ACS Catal.* 2017, **7**, 8006-8022.
10 N. E. Motl, A. F. Smith, C. J. DeSantis, S. E. Skrabalak, *Chem. Soc. Rev.* 2014, **43**, 3823-3834.
11 K. D. Gilroy, A. Ruditskiy, H.-C. Peng, D. Qin, Y. N. Xia, *Chem. Rev.,* 2016, **116**, 10414-10472.
12 X. Liu, M. T. Swihart, *Chem. Soc. Rev.,* 2014, **43**, 3908-3920.
13 F. J. García de Abajo, *ACS Photonics,* 2014, **1**, 135-152.
14 N. Jiang, X. Zhuo, J. Wang, *Chem. Rev.,* 2018, **118**, 3054-3099.
15 G. Y. Si, Y. H. Zhao, E. S. P. Leong, Y. J. Liu, *Materials,* 2014, **7**, 1296-1317.
16 K. Chen, E. S. P. Leong, M. Rukavina, T. Nagao, Y. J. Liu, Y. B. Zheng, *Nanophotonics,* 2015, **4**, 186-197.
17 O. Andreussi, S. Caprasecca, L. Cupellini, Guarnetti-Prandi, I.; C. A. Guido, S. Jurinovich, L. Viani, B. Mennucci, *J. Phys. Chem. A,* 2015**, 119**, 5197−5206.
18 Y. Zhang, S. He, W. Guo, Y. Hu, J. Huang, J. R. Mulcahy, W. D. Wei, *Chem. Rev.* 2018, **118**, 2927-2954.
19 N. J. Halas, S. Lal, W. S. Chang, S. Link, P. Nordlander, *Chem. Rev.,* 2011, **111**, 3913-3961
20 R-B. Wei, P.-Y. Kuang, H. Cheng, Y.-B. Cheng, J.-B. Long, M.-Y. Zhang, Z.-Q. Liu, *ACS Sustainable Chem. Eng.,* 2017, **5**, 4249−4257; Y.-C. Yen, J.-A. Chen, S. Ou, Y.-S. Chen, K.-J. Lin, *Scientific Reports,* 2017, **7**, 42524.
21 F. Wang, C. H. Li, H. J. Chen, R. B. Jiang, L.-D. Sun, Q. Li, J. F. Wang, J. C. Yu, C.-H. Yan, *J. Am. Chem. Soc.*, 2013, **135**, 5588-5601; M. D. Xiao, R. B. Jiang, F. Wang, C. H. Fang, J. F. Wang, J. C. Yu, *J. Mater. Chem. A*, 2013, **1**, 5790-5805.
22 K. Ueno, T. Oshikiri, Q. Sun, X. Shi, H. Misawa, *Chem. Rev.,* 2018, **118**, 2955-2993.
23 J.-M. Shi, L.-P. Mei; Q. Wang, W.-W. Zhao, J.-J. Xu, H.-Y. Chen, *Anal. Chem.,* 2018, **90**, 4277-4281; J. Xue, F. Chen, M. Bai, X. Yu, J. Wei, P. Huang, Y. Zhao, *ChemNanoMat,* 2017, **3**, 725 – 735.
24 J. Li, J. Liu, C. Chen, *ACS Nano,* 2017, **11**, 2403−2409; X. Yang, M. Yang, B. Pang, M. Vara, Y. Xia, *Chem. Rev.,* 2015, **115**, 10410−10488.
25 N. J. Halas, S. Lal, W.-S. Chang, S. Link, P. Nordlander, *Chem. Rev.,* 2011, **111**, 3913-3961; M. R. Jones, K. D. Osberg, R. J. Macfarlane, M. R. Langille, C. A. Mirkin, *Chem. Rev.,* 2011, **111**, 3736-3827.
26 A. Agrawal, S. M. Sho, O. Zandi, S. Ghosh, R. W. Johns, D. J. Milliron, *Chem. Rev.,* 2018, **118**, 3121-3207.
27 A. P. Upadhyay, D. K. Behara, G. P Sharma, M. Gyanprakash, R. G. S. Pala, S. Sivakumar, *ACS Sustainable Chem. Eng.,* 2016, **4**, 4511-4520.
28 L. Sang, Y. Zhao, C. Burda, *Chem. Rev.,* 2014, **114**, 9283-9318.
29 P. D. Ortiz, J. Castillo-Rodriguez, X. Zarate, R. Martin-Trasanco, M. Benito, I. Mata, E. Molins, E. Schott, *Langmuir,* 2018, **34**, 9402-9409.
30 M. Brust, M. Walker, D. Bethell, D. J. Schiffrin, R. Whyman, *J. Chem. Soc., Chem. Commun.* 1994, 801−802.
31 T. Hansen, K. Žídek, K. Zheng, M. Abdellah, P. Chábera, P. Persson, T. Pullerits, *Phys. Chem. Lett*. 2014, **5**, 1157−1162.
32 K. Kamata, K. Maeda, D. L. Lu, Y. Kako, K. Domen, *Chem. Phys. Lett.,* 2009, **470**, 90–94.
33 F. Guzman, S. S. C. Chuang, C. Yang, *Ind. Eng. Chem. Res.,* 2013, **52**, 61-65.
34 Y. Tamaki, A. Furube, M. Murai, K. Hara, R. Katoh, M. Tachiya, *J. Am. Chem. Soc.,* 2006, **128**, 416-417.
35 K. M. Mayer, J. H. Hafner, Localized Surface Plasmon Resonance Sensors. *Chem. Rev.,* 2011, **111**, 3828–3857.
36 T. Tachikawa, T. Yonezawa, T. Majima, *ACS Nano,* 2013, **7(1)**, 263-274.
37 C. G. Silva, R. Juárez, T. Marino, R. Molinari, H. García, *J. Am. Chem. Soc.* 2011, **133 (3)**, 595-602.
38 R. Kitamura, L. Pilon, M. Jonasz, *Applied optics*, 2007, **46(33)**, 8118-8133.
39 M. Kapilashrami, Y. Zhang, Y.-S. Liu, A. Hagfeldt, J. Guo, *Chem. Rev.,* 2014, **114**, 9662-9707.
40 J. R. Adleman, D. A. Boyd, D. G. Goodwin, D. Psaltis, *Nano Lett.,* 2009, **9**, 4417–4423.
41 E. Kowalska, O. O. P. Mahaney, R. Abe, B. Ohtani, *Phys. Chem. Chem. Phys.,* 2010, **12**, 2344–2355.
42 D. B. Ingram, S. Linic, *J. Am. Chem. Soc.,* 2011, **133**, 5202–5205.
43 C. di Valentin, G. Pacchioni, A. Selloni, *J. Phys. Chem. C*, 2009, **113**, 20543–20552.
44 N. Wang, T. Tachikawa, T. Majima, *Chem. Sci.,* 2011, **2**, 891–900.
45 H. M. Chen, C. K. Chen, C.-J. Chen, L.-C. Cheng, P. C. Wu, B. H. Cheng, Y. Z. Ho, M. L. Tseng, Y.-Y. Hsu, T.-S. Chan, *et al. ACS Nano*, 2012, **6**, 7362–7372.

View Article Online
DOI: 10.1039/D0NJ03250F

46 M. Valenti, M. P. Jonsson, G. Biskos, A. Schmidt-Otta, W. A. Smith *J. Mater. Chem. A*, 2016, **4**, 17891.
47 M. A. Khan, M. Al-Ouf, A. Toseef, M. A. Nadeem, H. Idriss *Catal Lett*, 2018, **148**, 1–10.
48 L. Martínez, M. Benito, I. Mata, L. Solera, E. Molins, J. Llorca. *Sustain. Energ. Fuels*, 2018, **2**, 2284-2295.
49 T. K. Rahul, M. Mohan, N. Sandhyarani *ACS Sustain. Chem. Eng.* 2018, **6**, 3049-3059.
50 L. Li, J. Yan, T. Wang, Z.-J. Zhao, J. Zhang, J. Gong, N. Guan *Nat. Commun.* 2015, **6**, 5881.
51 Z. Lian, W. Wang, G. Li, F. Tian, K. S. Schanze, H. Li, *ACS Appl. Mater. Inter.* 2017, **9** (20), 16959-16966
52 Y. Xu, C. Du, J. D. Steinkruge, C. Zhou, S. Yang *J. Mater. Sci.*, 2019, **54**, 6930–6942.
53 J. Schneider, M. Matsuoka, M. Takeuchi, J. Zhang, Y. Horiuchi, M. Anpo, D. W. Bahnemann, *Chem. Rev.,* 2014, **114**, 9919-9986.
54 M. Nazim, J. H. Kim**,** *ACS Omega*, 2020, **5**, 26, 16106–16119.
55 V. R. Akshay, B. Arun, G. Mandal, M. Vasundhara *Phys. Chem. Chem. Phys.,* 2019, **21**, 12991-13004.
56 B. Choudhury, B. Borah, A. Choudhury *Photochem. Photobiol.*, 2012, **88**, 257-264.
57 S. K. Khore, S. R. Kadam, S. D. Naik, B. B. Kale, R. S. Sonawane, *New J. Chem.,* 2018, **42**, 10958-10968.
58 L. Carlini, C. Fasolato, P. Postorino, I. Fratoddi, I. Venditti, G. Testa, C. Battocchio, *Colloids and Surfaces A,* 2017, **532**, 183–188.

View Article Online
DOI: 10.1039/D0NJ03250F

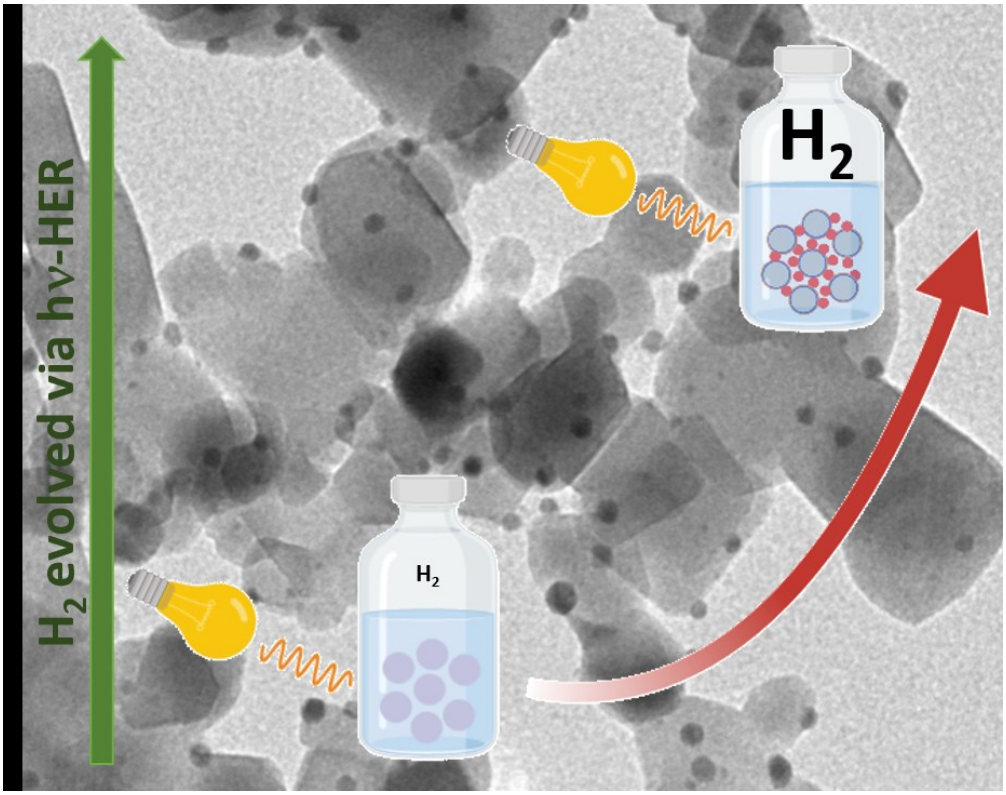

156x123mm (150 x 150 DPI)